The Astrophysical Journal, 682:697–705, 2008 July 20

THE LIFETIME OF ICE ON MAIN BELT ASTEROIDS

Norbert Schorghofer
Institute for Astronomy and NASA Astrobiology Institute, University of Hawaii, 2680 Woodlawn Drive, Honolulu, HI 96822
Received 2008 January 31; accepted 2008 March 27

ABSTRACT

We theoretically estimate the loss rate of buried ice from spherical bodies 2–3.3 AU from the Sun. The loss rate is explored as a function of about a dozen parameters. We introduce the concept of a "buried snow line," where the loss of ice is sufficiently slow over the age of the solar system. For a dusty surface layer, ice can persist within the top few meters of the surface over billions of years, if the mean surface temperature is less than about 145 K. Variations in surface layer properties within a plausible range are unlikely to change this threshold temperature by more than 10 K. Longevity of ice in the shallow subsurface of asteroid 7968 Elst-Pizarro is plausible. Parameter regions for ice to survive over the age of the solar system exist for all of the main asteroid belt, but preferentially for large distances from the Sun and slowly rotating bodies with surfaces consisting of small particles, leading to low thermal conductivity and short molecular free paths. Rocky surfaces, in contrast to dusty surfaces, are rarely able to retain ice in the shallow subsurface.

Subject headings: astrobiology — comets: general — minor planets, asteroids

1. INTRODUCTION

In the early solar system, the density of water molecules was high enough to lead to the condensation of ice from the gas phase, at a temperature that depends on the gas density and defines the "snow line." Today, water is lost from icy bodies to space. Here, we estimate this loss rate for small bodies in the main asteroid belt. The lack of the hydration signature in the outer belt found on asteroids in the inner belt (Jones et al. 1990) and the outgassing observed in the form of comet tails (Hsieh & Jewitt 2006) are among the evidence for the existence of present-day ice within the asteroid belt.

Sublimation loss of exposed ice is too rapid to be sustainable over billions of years, while buried ice potentially persists much longer. Fanale & Salvail (1984) have pointed out that on extinct comets, ice may be accessible within 10 m of the surface. Later, Fanale & Salvail (1989) showed that ice could have survived in the shallow subsurface at the polar regions of Ceres for 4.5 Gyr.

In the early solar system, ice may have been heated or even melted as a result of radioactive decay (McSween et al. 2002). Here we only consider the ability of ice to survive under present-day conditions. We are interested in slow changes of volatile content, appropriate for bodies that have orbited the Sun many times. The resulting modeling problem is incomparably simpler than models of active comets (Prialnik et al. 2004).

Considerations of the transport of water molecules through the porous surface layer (§ 2.1) and of how this layer evolves with time (§ 2.2) lead to the concept of a "shallowly buried snow line" (§ 2.3). By way of example, with end-member thermal models and realistic models of temperature, it is easy to demonstrate that ground ice can survive on some bodies in the main asteroid belt (§§ 3.2 and 3.3), corroborating the results of Fanale & Salvail (1984, 1989). By systematically identifying how various parameters affect temperature, it is possible to obtain extreme but still realistic model scenarios which bracket plausible ranges of temperature; these calculations establish that ice can persist, and they reveal preferred orbital and physical parameters (§§ 3.3 and 3.4). After discussion of miscellaneous issues in § 4, the results are summarized in § 5. Frequently used symbols are defined in Table 1.

2. ICE LOSS PHYSICS

2.1. H_2O *Transport through Porous Media*

At temperatures below about 180 K, the mean free path of water molecules in otherwise empty space is more than 1 m, and therefore transport through a porous medium is by Knudsen diffusion. Kinetic theory suggests that the Knudsen diffusion coefficient $D_{\rm K}$ is given by (Mason et al. 1967)

$$D_{\rm K} = \frac{4}{3}\bar{v}K_0, \tag{1}$$

in which $\bar{v}$ is the mean thermal speed of the gas molecules and K_0 is a constant characteristic of the medium with units of length. For example, in a long straight circular capillary of radius r, the diffusion coefficient at low pressure is $D_{\rm K} = (2/3)\bar{v}r$ (Mason & Malinauskas 1983). The parameter K_0 is related to the molecular mean free path. For a porous medium, Evans et al. (1961) give the approximate relation

$$K_0 = \frac{9}{128}\frac{1}{1+\pi/8}\frac{\phi}{\tau}\frac{1}{n_d r^2}, \tag{2}$$

where r is the rms grain radius, ϕ is porosity, n_d is the number density of grains, and τ is tortuosity. Number density, porosity, and radius of spherical particles are by definition related by $n_d = 3(1-\phi)/(4r^3\pi)$. Combined with equation (1), the diffusion coefficient is

$$D_{\rm K} = \frac{\pi}{8+\pi}\frac{\phi}{1-\phi}\frac{\bar{v}r}{\tau}. \tag{3}$$

The mean thermal velocity is $\bar{v} = [8k_{\rm B}T/(\pi m)]^{1/2}$, where $k_{\rm B}$ is the Boltzmann constant and m is the molecule mass. The mean grain size in lunar soil samples is typically 45–100 μm (Heiken et al. 1991), which might also be representative for the surface layer of asteroids and comets. Many asteroids appear to have significant porosity (Britt et al. 2002). The diffusivity depends strongly on the free path available to molecules, and the mean

TABLE 1
NOTATION

Symbol	Meaning
A	Albedo
a	Semimajor axis
e	Orbital eccentricity
ϵ	Infrared emissivity
I	Thermal inertia
$\bar{J}$	Net mass flux of H_2O
k	Thermal conductivity
m	Mass of H_2O molecule
p_s	Equilibrium vapor pressure of H_2O
r	Grain radius, also radius of capillary
T	Temperature
T_1	Surface temperature of fast-rotating thermal model
T_2	Surface temperature of standard thermal model
T_3	Surface temperature of full thermal model
Δz	Thickness of ice-free layer
δ	Latitude
θ	Obliquity
Ω	Solar longitude of perihelion relative to body's equinox

free path is the most variable and uncertain parameter for the diffusion coefficient.

The mass flux of H_2O molecules is given by

$$J = -D_K \frac{\partial \rho_v}{\partial z}, \tag{4}$$

where ρ_v is the vapor density and z is depth. When ice is present, the vapor density ρ_v is determined by the equilibrium vapor density ρ_s. The equilibrium vapor pressure p_s of crystalline ice is well known for temperatures above $\sim$150 K (Sack & Baragiola 1993; Bryson et al. 1974). The literature provides various expressions for the equilibrium vapor pressure of crystalline ice that closely agree with one another (Washburn et al. 2003; Bryson et al. 1974; Hardy 1998). Here, a constant sublimation enthalpy is used of the form

$$\ln \frac{p_s}{p_t} = -\frac{\Delta H}{R}\left(\frac{1}{T} - \frac{1}{T_t}\right), \tag{5}$$

where $\Delta H = 51.058$ MJ kg^{-1}, $p_t = 611$ Pa, $T_t = 273.16$ K, and R is the universal gas constant. Less understood is the vapor pressure of amorphous ice, and its presence at lower temperatures. Kouchi (1987) measured the vapor pressure of vapor-deposited amorphous ice to be 1 or 2 orders of magnitude larger than that of crystalline ice, but subsequent measurements showed a lower enhancement (Kouchi 1990; Sack & Baragiola 1993). Later, the sublimation rate was found to depend on the conditions under which the ice was grown (Sack & Baragiola 1993; Jenniskens et al. 1998; Baragiola 2003).

It is straightforward to apply equation (4) to an environment where temperature changes with time (see, e.g., Schorghofer 2007). The net flux from the subsurface ice through a porous soil layer of thickness Δz to empty space is

$$\bar{J} = -D_K \frac{\overline{\rho_s}}{\Delta z}, \tag{6}$$

where the overbar indicates time averages over one or more orbits. The depth Δz is the uppermost depth at which permanent ice exists. Equation (6) is not merely a rough estimate, but essentially an exact leading order description of the flux of molecules migrating through a porous layer that experiences spatially and temporally varying temperature.

Equations (3) and (6), combined with the ideal gas law $p_s = \rho_s k_B T/m$ yield

$$\bar{J} = \frac{2\pi}{8+\pi}\frac{\phi}{1-\phi}\frac{1}{\tau}\sqrt{\frac{2m}{\pi k_B T}}p_s \frac{r}{\Delta z}. \tag{7}$$

In the very same context, Fanale & Salvail (1984) using a model of capillary tubes of radius r, arrived at

$$\bar{J} = \frac{4}{9}\frac{\phi}{\tau^2}\sqrt{\frac{2m}{\pi k_B T}}p_s \frac{r}{\Delta z}. \tag{8}$$

Their formula differs from equation (7) only by a prefactor close to unity (Schorghofer & Taylor 2007).

Laboratory measurements of water vapor diffusion in porous media at the crossover range between Knudsen and Fickian diffusion (Hudson et al. 2007) demonstrate that simple theoretical estimates of diffusion coefficients are valid for loose dust and other soil simulants.

2.2. *Time Evolution of Surface Layer*

When a layer of pure ice recedes, its retreat rate is

$$R_i = \bar{J}/\rho_{\text{bulk ice}}, \tag{9}$$

where $\rho_{\text{bulk ice}} \approx 930$ kg m^{-3}. When the ice contains dust, the overlying layer will grow with time. The instantaneous loss rate R_i, which has units of speed, is used throughout this paper. For illustration, if we choose a particle diameter of 100 μm, a protective layer of 1 m thickness, a porosity of 0.5, and a tortuosity of 2, then the retreat rate at 150 K according to equations (7) and (9) is 9 m Gyr^{-1}.

Due to temperature fluctuations caused by a body's rotation and the orbit around the Sun, the surface experiences higher peak temperatures than ice at depth, which is protected from the temperature variations by the thermal skin effect. The time-averaged $\bar{\rho}_s$ for exposed ice is larger than for buried ice. As a result, ice will rapidly retreat to below the thermal skin depth. Thereafter, the loss rate is determined by the mean temperature, and the ice no longer contributes to the thermal properties of the surface layer within the influence of the annual skin depth.

When ice retreats, a sharp interface is maintained between an essentially ice-free sublimation lag and the underlying ice-rich layer, such that the above expressions for the flux remain applicable even after a long time. Ice is lost to space by recession of the uppermost ice boundary. If there are pathways for molecules to migrate within the ice-rich layer, then H_2O can be redistributed when driven by temperature gradients, but without a geothermal gradient no net migration takes place. For the low temperatures relevant here, the latent heat of sublimation is negligible.

If ice-rich bodies formed within the main asteroid belt, and if these bodies were not significantly heated by radioactive decay in their interior or by major external events, then the presence of water ice is determined by the rate of ice loss. The ice may be interstitial in a regolith matrix that remains after the ice is depleted or, if the fraction of nonvolatile material contained in water ice is small, a lag will form. If material is contained within the ice, the dry surface layer grows as the ice recedes. If the dust content is sizable, the rate at which the dry layer grows and the rate R_i at which ice recedes are of the same order of magnitude. For ice to

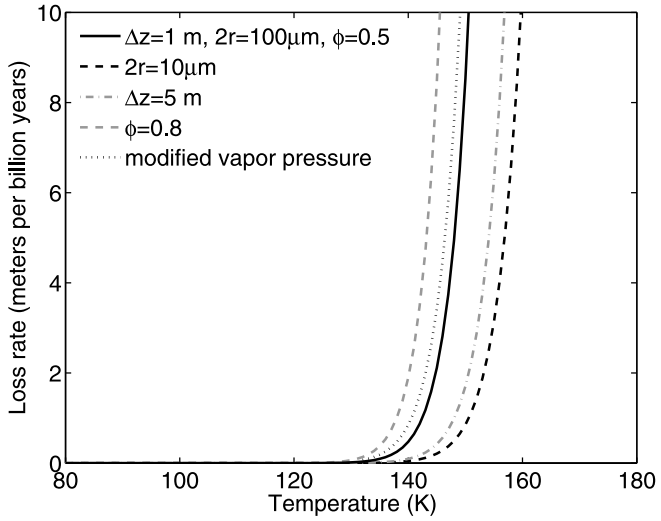

FIG. 1.—Theoretical loss rates for ice buried by material of thickness Δz with grain radius r and porosity ϕ. The solid black line is a reference case with parameters listed in the first legend entry. For the other line types, the legend indicates the parameter which differs from the reference case. The calculations use the equilibrium vapor pressure for crystalline ice, but one graph with a modified vapor pressure, from Bryson et al. (1974), is also shown, where $\ln p_s = -\Delta H/(RT) + 21.7$ (in torr) and $\Delta H = 11.4$ kcal mol^{-1} for 132–153 K.

survive in the shallow subsurface, the loss rate should be no more than a few meters per billion years.

2.3. *The Buried Snow Line*

The parameters that influence ice loss are diffusion coefficient (which in turn largely depends on grain size), burial depth, and temperature. The vapor density in the vicinity of ice depends very strongly on temperature, because temperature enters close to exponentially in $p_s(T)$. At 145 K, the vapor density changes by a factor of 2 when temperature varies by ± 2.5 K, and it changes by a factor of 10 within about ± 9 K.

Figure 1 shows the loss rate from equations (7) and (9) for various parameters as a function of temperature. The solid line shows a reference case, ice beneath a 1 m thick layer of 100 μm grains. The other graphs differ from the reference case in one parameter each to demonstrate the variability in loss rate due to incomplete knowledge of the physical environment. The tortuosity is 2 in all cases. The plot purposely shows the loss rate on a linear axis, and the temperature range is not as wide as the temperature distribution expected for asteroid surfaces. The figure demonstrates that varying parameters within a reasonable range corresponds to no more than 10 K change in temperature. Temperature dwarfs all other parameter dependencies.

It is now apparent that prolonged survival of ice requires sufficiently low temperature. For the parameters considered in Figure 1, it is reasonable to demand that temperature stays below 145 K. Depending on the nature of the surface layer, this temperature may be 135–155 K. At 160 K it would be difficult for any protective layer to maintain ice in the topmost meter of the surface for billions of years. Likewise, retreat rates at 130 K are so small that ice should have survived for almost any type of dusty surface layer. (A 10% reduction in solar luminosity corresponds to a $\sim$4 K temperature decrease.)

The considerations so far enable us to introduce the concept of a "buried snow line." Within order-of-magnitude considerations of loss rates, there is a well-defined temperature, a narrow temperature range, which realistically determines whether ice can survive in the shallow subsurface for billions of years, even in light of uncertainty about other parameters. This effectively defines a fairly sharp longevity boundary expressed as a temperature.

The existence of a buried snow line can be compared with the phenomenon of ice in permanently shaded areas on Mercury and the Moon (Watson et al. 1961). The loss rate E into vacuum, in units of mass per area and time, is

$$E = p_s \sqrt{\frac{m}{2\pi k_B T}}. \tag{10}$$

At 120 K the sublimation loss into vacuum is on the order of 10 m Gyr^{-1}. The ratio of equation (10) with the loss rate of buried ice, equation (7), involves a factor of $r/\Delta z$. This ratio brings the relevant threshold temperature from 120 to 145 K.

The buried snow line is only an approximate concept. It is possible to invalidate it when the free path for molecules to escape is orders of magnitude larger than 100 μm. Likewise, it is possible that the surface layer is not meters but kilometers thick. The dependence on layer thickness can be essentially removed by refining the concept. In the context of main belt comets, we are interested in the top few meters of the surface, and hence a "shallowly buried snow line." On the other hand, for the total ice content of a large body, even ice buried 1 km may be relevant. In this case, we can speak of a "deeply buried snow line." The temperature boundary for a deeply buried snow line is about 170 K, accounting for the 3 orders of magnitude slower diffusion loss caused by a kilometer-thick protective layer compared to a meter-thick protective layer with similar physical properties. Since the material may be less porous at greater depth, the temperature boundary for the deeply buried snow line may be even higher, and it is more difficult to estimate than the shallowly buried snow line.

3. TEMPERATURE MODELS

As argued above, the mean temperature is the most important parameter for the loss rate of ice. At sufficient depth, temperature does not vary with time and is independent of the position of the body along its orbit. Nevertheless, the amount of radiation from the body depends strongly on peak surface temperature, and thus on the thermal properties near the surface.

3.1. *Thermal Inertia*

The thermal conductivity k of lunar regolith determined from Apollo experiments is $(0.9–1.3) \times 10^{-2}$ W m^{-1} K^{-1} (Langseth et al. 1976). The bulk density of small comets is lower than the density of the lunar surface layer, suggesting their conductivity is less. Presley & Christensen (1997a) review thermal conductivity measurements and theory for particulate materials. In a vacuum, typical values are on the order of 10^{-2} W m^{-1} K^{-1}. In their own experiments, Presley & Christensen (1997b) find empirically that the thermal conductivity is proportional to the square root of particle size. In these experiments, for particles 10–100 μm in size, k is less than 10^{-2} W m^{-1} K^{-1}, and an atmosphere of 1 torr still contributes to heat conduction, which implies that the conductivity in vacuum is lower. Assumed thermal conductivity values for cometary dust, as reviewed by Prialnik et al. (2004) are 0.1–4 W m^{-1} K^{-1}, substantially larger than those measured in the laboratory and on the Moon. A reasonable value given the aforementioned laboratory experiments and lunar measurements is $k = 10^{-3}$ W m^{-1} K^{-1}.

Thermal inertia is defined by $I = (k\rho c)^{1/2}$, where ρ is density and c is heat capacity. With $k = 10^{-3}$ W m^{-1} K^{-1}, $\rho = 500$ kg m^{-3}, and $c = 800$ J kg^{-1} K^{-1}, the inertia is $I = 20$ J m^{-2} K^{-1} s$^{-1/2}$. The thermal skin depth is $I/(\rho c)(P/\pi)^{1/2}$, where P is the time

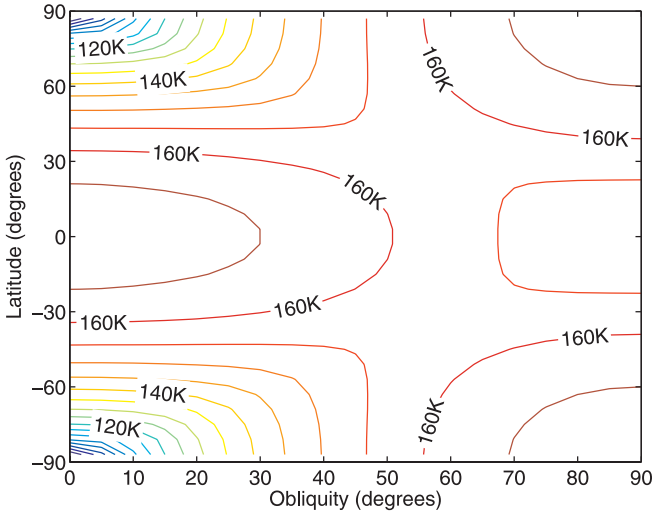

FIG. 2a

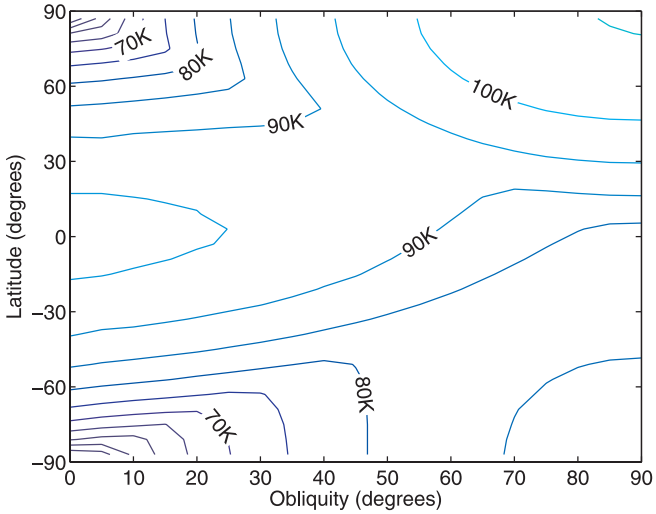

FIG. 2b

FIG. 2.—(*a*) Mean surface temperature of a spherical body for a fast rotating body or infinite thermal conductivity and a semimajor axis of 3.2 AU. Contours are spaced by 5 K. Polar regions on bodies with low obliquity remain below 145 K. The albedo is 0.05, the eccentricity 0.1, $\Omega = 250^\circ$, and the infrared emissivity 0.9. (*b*) Same as *a*, but for the opposite extreme of a slowly rotating body or zero thermal conductivity (also known as standard thermal model).

period of temperature oscillations. With these parameters, the skin depth for a 4 yr orbit is 0.3 m.

Spencer et al. (1989) argue that the thermal inertia of most main belt asteroids is less than 1.5×10^4 erg cm^{-2} K^{-1} s$^{-1/2}$ (15 J m^{-2} K^{-1} s$^{-1/2}$). The thermal inertia derived from temperature maps of comet 9P/Tempel 1, the most direct measurement available, is less than 50 J m^{-2} K^{-1} s$^{-1/2}$ (Groussin et al. 2007). A thermal conductivity on the order of 10^{-3} W m^{-1} K^{-1} is consistent with these observational measurements. These values are typical for dusty and not for rocky surfaces.

In a vacuum at sufficiently high temperature, heat transfer is dominated by radiation instead of conduction. Thermal conductivity therefore depends on temperature. A model for the top layer of the lunar surface takes the temperature dependence of the thermal conductivity as $k = k_c[1 + \chi(T/350)^3]$, with $k_c = 9.22 \times 10^{-4}$ W m^{-1} K^{-1} and $\chi = 1.48$ (Cremers & Birkebak 1971; Vasavada et al. 1999). An expression for the temperature dependence of heat capacity, based on lunar samples, is given in Ledlow et al. (1992). At temperatures 50, 150, and 250 K the heat capacity is 112, 434, and 672 J kg^{-1} K^{-1}, respectively. Assuming a density of 500 kg m^{-3}, the resulting thermal inertias are 7.2, 15, and 22 J m^{-2} K^{-1} s$^{-1/2}$, respectively. This exemplifies the change in thermal inertia with temperature.

3.2. *End-Member Thermal Models*

Before going into full thermophysical calculations, we consider two end-member thermal models (Lebofsky & Spencer 1990).

The first of these models assumes a surface element remains at constant temperature over diurnal and seasonal cycles or has infinite thermal inertia. This is also known as the fast-rotating or isothermal latitude model (Lebofsky & Spencer 1990). This equilibrium temperature T_1 is determined by

$$(1 - A)\bar{Q} = \epsilon\sigma T_1^4, \tag{11}$$

where A is albedo, $\bar{Q}$ is the mean of the incoming solar flux, ϵ is the infrared emissivity, and σ is the Stefan-Boltzmann constant. The temperature T_1 is constant with time and can be obtained by averaging the incoming solar flux over one orbit around the Sun. The instantaneous flux Q thereby depends on heliocentric distance and solar incidence angle, and it vanishes on the night side. Distance and declination of the Sun in planetocentric coordinates are computed from orbital elements using standard astronomical formulas. The incidence angle for a given latitude is calculated from declination and hour angle.

Results for the temperature T_1, from numerical averaging of Q, are shown in Figure 2*a* for a spherical body 3.2 AU from the Sun. The semimajor axis of the three known main belt comets (MBCs) is 3.16–3.20 AU. Polar areas of bodies with low obliquity have a mean temperature of less than 145 K, but when the body is not spherical, polar temperatures might not be that low.

The model can in fact be solved analytically. Ward (1974) gives the mean annual insolation at latitude δ as

$$\bar{Q} = \frac{1}{2\pi^2}\frac{S_0}{a^2}\frac{1}{\sqrt{1-e^2}} \times \int_0^{2\pi} \sqrt{1 - (\sin\delta\cos\theta - \cos\delta\sin\theta\sin\varphi)^2}\, d\varphi, \tag{12}$$

where S_0 is the solar constant, a is the semimajor axis in AU, e is eccentricity, and θ is obliquity. The annual mean does not depend on the longitude of the perihelion, and it depends on eccentricity only beyond first order. At the poles, $\bar{Q} = (S_0/a^2)\sin\theta/[\pi(1 - e^2)^{1/2}]$, and the resulting temperature as a function of θ is in excellent agreement with our numerical results.

The other end-member is represented by the nonrotating or standard thermal model, which assumes an instantaneous equilibration of surface temperature or zero thermal inertia:

$$(1 - A)Q = \epsilon\sigma T_2^4. \tag{13}$$

The average surface temperature $\bar{T}_2$ can again be obtained directly from Q with purely geometrical calculations along a single orbit, but they represent lower than realistic temperatures. Figure 2*b* shows that at 3.2 AU the standard thermal model mean surface temperatures, $\bar{T}_2$, are always below 145 K for all obliquities and latitudes.

From the large difference in mean temperatures in these two end-member thermal models (cf. Figs. 2*a* and 2*b*), it is apparent that rotation period and thermal inertia are important parameters

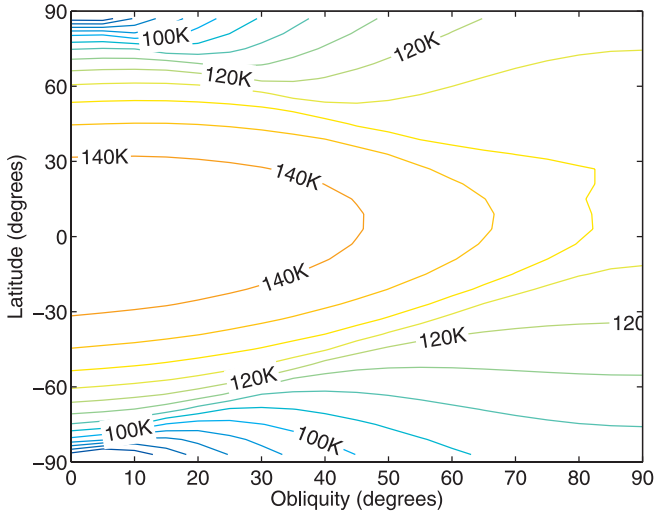

FIG. 3a

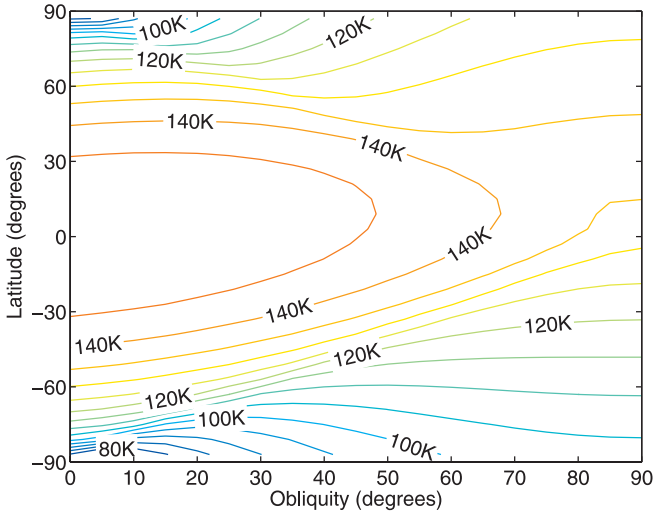

FIG. 3b

FIG. 3.—(*a*) Mean surface temperatures of a rotating spherical body 3.2 AU from the Sun. The thermal inertia is 10 J m^{-2} K^{-1} s$^{-1/2}$ and the rotational period 10 hr. At this distance and rotation rate, the entire surface remains below an annual mean of 145 K. (*b*) Mean surface temperatures of a spherical body with the orbital elements and rotation period of main belt comet 133P/Elst-Pizarro. The thermal inertia is assumed to be 10 J m^{-2} K^{-1} s$^{-1/2}$.

in the problem. Nevertheless, since the "hot" end-member calculation of Figure 2*a* still includes parameter regions with a buried snow line, it is clear that ground ice is able to survive over the age of the solar system at some locations.

3.3. *Realistic Temperature Calculations*

A body with finite thermal conductivity and rotation rate requires subsurface conduction be added to the model,

$$(1 - A)Q = \epsilon\sigma T^4 + k\frac{\partial T}{\partial z}, \tag{14}$$

$$\rho c\frac{\partial T}{\partial t} = \frac{\partial}{\partial z}\left(k\frac{\partial T}{\partial z}\right), \tag{15}$$

where z is depth and t is time. Lateral heat transport is assumed to be negligible, and briefly discussed in § 4. This model has two invariants that reduce the number of independent parameters (Lebofsky & Spencer 1990). The surface temperature only depends on the combination of parameters $I = (\mathrm{k}\rho\mathrm{c})^{1/2}$. Second, as long as the rotation period is much shorter than the orbital period, the result is the same when $\omega^{1/2}I$ is the same, where $\omega = 2\pi/P_{\mathrm{rot}}$ and P_{rot} is the length of a solar day. Both invariances are violated when thermal conductivity of the surface layer depends on temperature, as it does for radiative heat transfer.

Equations (14) and (15) are solved numerically with a Cranck-Nicholson scheme using geometrically spaced depths from the surface down to five orbital skin depths and a sufficient number of grid points within the rotational skin depth (typically six). The heat flux from the interior is assumed to be zero. The thermal propagation is evolved for 10 orbits to equilibrate, and averages are taken over the 11th orbit. There are 50 time steps for every solar day. Despite the discussion in § 3.1, thermal inertia is taken to be independent of temperature, for reasons that will become apparent below.

Figure 3*a* shows mean surface temperatures assuming $I = 10$ J m^{-2} K^{-1} s$^{-1/2}$, a rotation period of 10 hr, and a semimajor axis of 3.2 AU. The mean temperature is below 145 K on the entire surface. For comparison, Figure 2*a* shows calculations for $I\omega^{1/2} = \infty$ and Figure 2*b* represents the limit $I\omega^{1/2} = 0$. Figure 3*a* corresponds to a realistic value of $I\omega^{1/2} = 0.13$ W m^{-2} K^{-1}. The temperatures for the fast-rotating model in Figure 2*a* are on average 30 K warmer than the more realistic temperatures of Figure 3*a*, and the standard model temperature of Figure 2*b* are an average of 37 K colder, such that neither of the two end-member thermal model provides reasonable temperature estimates.

Figure 3*b* shows model results with the orbital elements of asteroid 7968 Elst-Pizarro, also known as comet 133P/Elst-Pizarro. Its rotation rate is known to be 3.5 hr (Hsieh et al. 2004), but thermal inertia and the longitude of the body's equinox need to be assumed. The hemispheric asymmetry in Figure 3 arises from the arbitrary choice of Ω. We conclude that it is perfectly plausible that ice has survived within the shallow subsurface at the distance of known main belt comets.

Elst-Pizarro appears to be significantly elongated based on its light curve (Hsieh et al. 2004; Toth 2006). In the special case of a prolate spheroid rotating around its major axis (or an oblate spheroid rotating around its minor axis), the temperatures of Figure 3*b* remain applicable if the latitude is measured between the equator and the normal to the surface (planetodetic latitude). Deviations between the calculated temperatures and that of an elongated and irregularly shaped body are expected, but a larger uncertainty lies in the thermal inertia of the surface.

A quantity of interest is the fraction of surface area colder than the threshold temperature of 145 K. After mean temperatures are calculated for the entire surface, the area fraction is obtained by counting all latitudes where mean temperature is less than the threshold temperature, weighing with the cosine of latitude. Figure 4 shows results using mean surface temperatures for $I = 10$ J m^{-2} K^{-1} s$^{-1/2}$ and 5000 rotations per orbit (depending on distance 5.0–10.5 hr). It involves calculations at many distances, obliquities, and latitudes that are carried out on a computer cluster. At a distance of 2 AU only polar areas of bodies with low obliquity have a mean temperature of less than 145 K. At distances beyond 3.2 AU, all of the surface is below 145 K for any obliquity. Bodies with high obliquity have the largest fraction of their surface below the threshold temperature of 145 K, although according to Figure 3 the lowest temperatures are found at low obliquity.

The thermal inertia and rotation period of asteroid Ceres are comparable to what is assumed in the calculations for Figure 4.

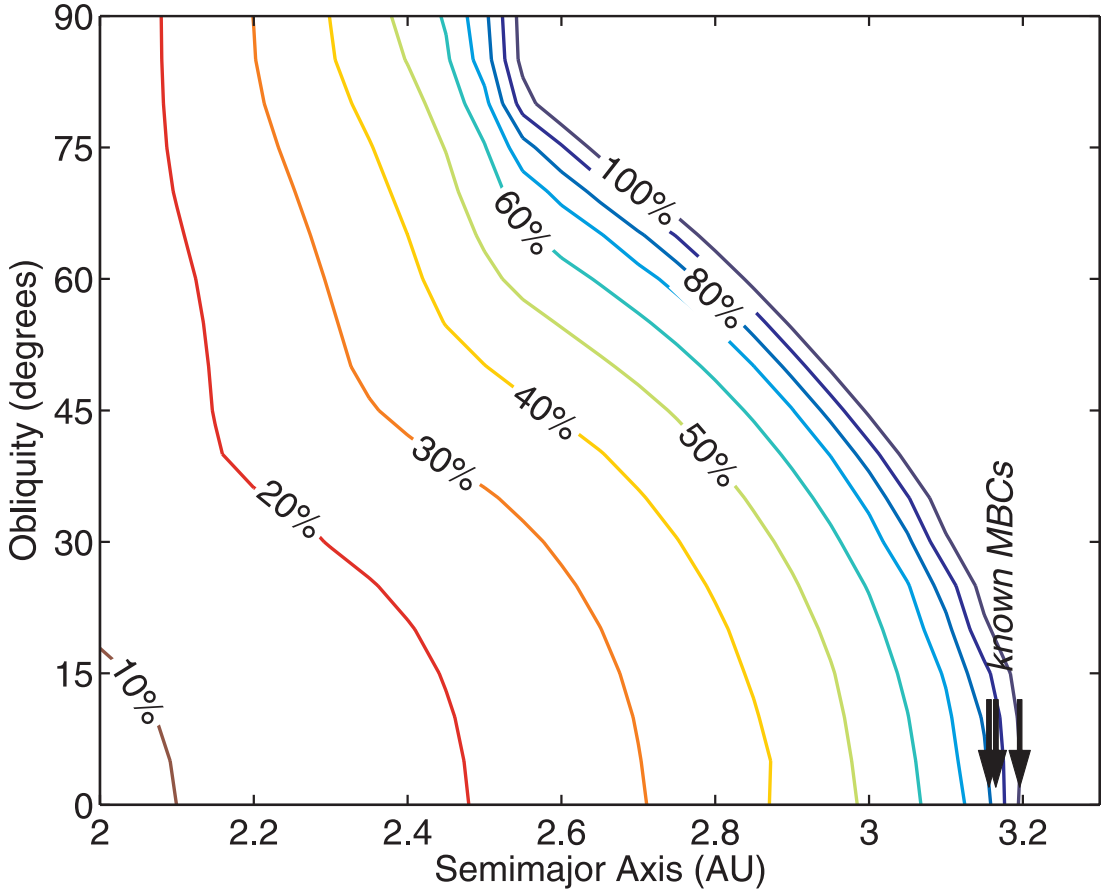

FIG. 4.—Contours show the fraction of surface area of a spherical body where the mean temperature is below 145 K. The thermal inertia is 10 J m^{-2} K^{-1} $s^{-1/2}$, and the rotational period is 1/5000th of the orbital period. This plot is based on thermal calculations for 16,200 different combinations of semimajor axis, obliquity, and latitude. The albedo is 0.05, the eccentricity 0.1, $\Omega = 250^\circ$, and the infrared emissivity 0.9. The semimajor axes of the known main belt comets 133P/Elst-Pizarro, P/2005 U1 (Read), and 118401 (1999 RE_{70}) are also shown.

Ceres has an obliquity close to zero and a semimajor axis of 2.77 AU, such that its polar regions may have been able to retain ice in the shallow subsurface.

These estimates show that mean temperatures can be low enough for subsurface ice to survive over the age of the solar system in all of the main belt, but preferentially for large distances, slowly rotating bodies, and low thermal conductivity. While the coldest spots exist at low obliquity, it is high obliquity that it is more likely to bring the entire surface below the buried snow line temperature.

3.4. *Parameter Dependence of Temperature*

The sensitivity of mean surface temperature to various parameters is explored in Table 2. In both the top and bottom sections of the table, the first row is a reference calculation that other temperatures are compared with ($\Delta\bar{T}$ in col. [7]). According to the considerations in § 2.3, for the loss rate to be correctly estimated within 1 order of magnitude, mean temperature needs to be known within 9 K, or less to also allow for variations in other unknown parameters. According to Table 2, most parameters cause variations of only a few kelvins. The parameters $P_{\rm rot}$ and I can vary over such a large range that their influence on equatorial mean temperature can be substantial (Table 2, top). For an obliquity of 20°, the temperature in polar latitudes depends less on rotation period but notably on eccentricity (Table 2, bottom). The last row in each section of the table shows a model calculation where thermal conductivity and heat capacity vary with temperature, as described in § 3.1. The model temperatures barely differ from the reference case, such that variable thermal properties do not need to be taken into account, as long as the thermal inertia is representative for mean temperature.

Temperature clearly depends monotonically on A, ϵ, $P_{\rm rot}$, and I. The dependence on the orbital eccentricity e requires additional thought. In the analytic expression (12) for one of the end-member thermal models, eccentricity only enters to second order, and the mean temperature increases with eccentricity for all obliquities and latitudes. This is borne out in Table 2, for the end-member temperature T_1 as well as the more realistic model temperature $\bar{T}_3$. At different obliquity, the dependence of $\bar{T}_3$ on e can have the opposite sign, as seen in the equatorial temperature of Table 3, where the more eccentric orbit leads to a small temperature drop compared to the circular orbit. At higher latitudes, $\bar{T}_3$ still increases with e. Hence, $\bar{T}_3$ generally increases with e, although not always, but the observed decrease is very small.

Guided by the results of Tables 2 and 3, we can further study the uncertainty in temperature due to incomplete knowledge of the body's properties by using a "warm case" ($I = 25$ J m^{-2} K^{-1} $s^{-1/2}$, $P_{\rm rot} = 2$ hr, $A = 0.04$, $\epsilon = 0.9$, and $e = 0.25$) and a "cold case" ($I = 5$ J m^{-2} K^{-1} $s^{-1/2}$, $P_{\rm rot} = 40$ hr, $A = 0.2$, $\epsilon = 1$, and $e = 0$). The two rotation rates bracket that of most asteroids (Pravec et al. 2002). Figure 5 shows again the fraction of the area of a spherical body colder than 145 K. These two extremes bracket a far more reasonable temperature range than the two end-member thermal models discussed above. The end-member models only represent theoretical extremes in thermal inertia and rotation rate. The two cases in Figure 5 still represent extremes, as every parameter

TABLE 2
PARAMETER DEPENDENCE OF SURFACE TEMPERATURE

A (1)	ϵ (2)	e (3)	P_{rot} (hr) (4)	I (J m^{-2} K^{-1} s$^{-1/2}$) (5)	$\bar{T}_3$ (K) (6)	$\Delta\bar{T}$ (K) (7)	T_1 (K) (8)	$\bar{T}_2$ (K) (9)	Comment (10)
				Latitude $\delta = 0^\circ$					
0.05	0.9	0.1	9.11	10	148	...	172	99	
0.20	0.9	0.1	9.11	10	143	−5	165	94	
0.05	*1.0*	0.1	9.11	10	144	−4	168	96	
0.05	0.9	*0*	9.11	10	148	0	172	99	
0.05	0.9	*0.2*	9.11	10	148	0	173	98	
0.05	0.9	0.1	*2.28*	10	154	+6	172	99	
0.05	0.9	0.1	*36.4*	10	142	−6	172	99	
0.05	0.9	0.1	9.11	*50*	162	+14	172	99	
0.05	0.9	0.1	9.11	10[a]	148	0	172	99	T-dependent
				Latitude $\delta = 80^\circ$ N					
0.05	0.9	0.1	9.11	10	105	...	134	83	
0.20	0.9	0.1	9.11	10	102	−4	129	79	
0.05	*1.0*	0.1	9.11	10	103	−3	131	81	
0.05	0.9	*0*	9.11	10	100	−5	134	76	
0.05	0.9	*0.2*	9.11	10	111	+5	135	90	
0.05	0.9	0.1	*2.28*	10	107	+1	134	83	
0.05	0.9	0.1	*36.4*	10	104	−1	134	83	
0.05	0.9	0.1	9.11	*50*	113	+7	134	83	
0.05	0.9	0.1	9.11	10[a]	104	−1	134	83	T-dependent

NOTE.—The semimajor axis is 3 AU, the obliquity 20°, and $\Omega = 250^\circ$ in all cases. Italics highlight the parameter that is changed relative to the reference case in the first row.
[a] Thermal inertia at 150 K.

is changed to decrease or increase the temperature, respectively, such that it is likely that most dust-mantled main belt asteroids fall in between these two cases. This in turn implies that longevity of ice should be commonplace on bodies within the range of properties considered here.

3.5. *Rocky Surfaces*

Ice loss from rocky surfaces proceeds much faster than from dusty surfaces for several reasons. The thermal conductivity of large rocks is higher than that of small grains, which increases mean surface temperature. Model calculations for $I = 200$ J m^{-2} K^{-1} s$^{-1/2}$, still less than a purely rocky surface, are carried out with all other parameters as given in the caption of Figure 4. Mean surface temperatures differ on average by 20 K from $I = 10$ J m^{-2} K^{-1} s$^{-1/2}$. This demonstrates that the thermal component alone is substantial. Moreover, the thermal skin depth for $I = 200$ J m^{-2} K^{-1} s$^{-1/2}$ increases to meters, such that retreat rates in the shallow subsurface are higher than for mean temperature.

TABLE 3
SURFACE TEMPERATURE DEPENDENCE ON ECCENTRICITY

δ (deg)	e	$\bar{T}_3$ (K)	T_1 (K)	$\bar{T}_2$ (K)
0	0	137	159	90
	0.3	136	161	89
30	0	130	162	91
	0.3	141	164	107
80	0	119	170	97
	0.3	141	172	126

NOTE.—The obliquity is 70°, and all other parameters are as in the reference cases of Table 2.

The molecular free path is much larger than for small grains. Should the particle size be 1 cm instead of 0.1 mm and the voids correspondingly larger, then according to equation (7) the buried snow line temperature drops from 145 to 130 K. The model calculations for $I = 200$ J m^{-2} K^{-1} s$^{-1/2}$ and a temperature threshold of 130 K reveal that ice is rarely long lived, as seen in Figure 6.

4. DISCUSSION

For illustration, we can consider retreat rates not as a function of temperature, as in Figure 1, but as a function of latitude using the orbital elements of main belt comet 133P/Elst-Pizarro. Figure 7 shows surface temperature, averaged over one orbit, and resulting retreat rates. The retreat rates are again shown for various physical properties of the surface layer. The buried snow line is not as well defined in latitude as it is in temperature. The high latitudes are undoubtedly areas of ice longevity, while at equatorial regions ice may retreat to greater depth or remain near the surface, depending on the properties of the surface layer. The variability of layer properties on a single body is likely less than considered in the lower panel of Figure 7, such that the latitudinal boundary is likely still fairly well defined.

The spin axis orientation of asteroids, to the extent known, is not isotropically distributed (Pravec et al. 2002; Kryszczynska et al. 2007). Moreover, obliquity and spin rotation period can change through collisions, Yarkovsky effect, and YORP effect. When the rotation axis of the body tumbles or wobbles, then the warmest temperature limits the lifetime of ice, as ice is lost quickly when no longer close to the buried snow line temperature. Depending on rotation rate and thermal inertia, ice will survive tumbling at sufficiently large distances from the Sun (as in Fig. 5*a* beyond 2.25 AU) or not (as in Fig. 5*b*). The chance of survival increases with distance from the Sun.

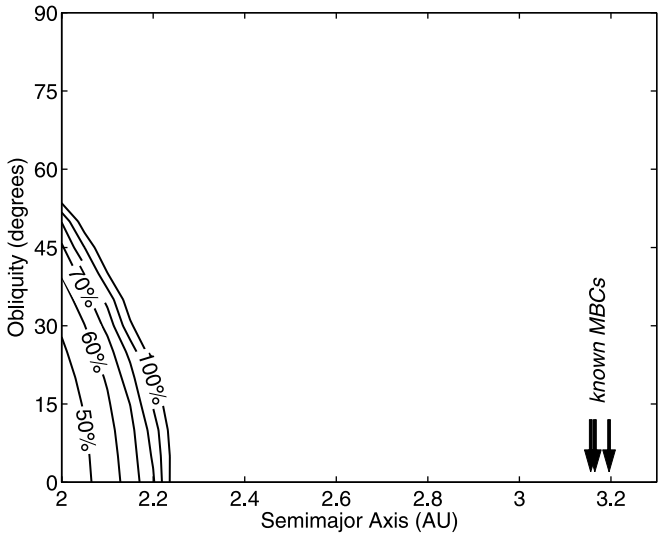

FIG. 5a

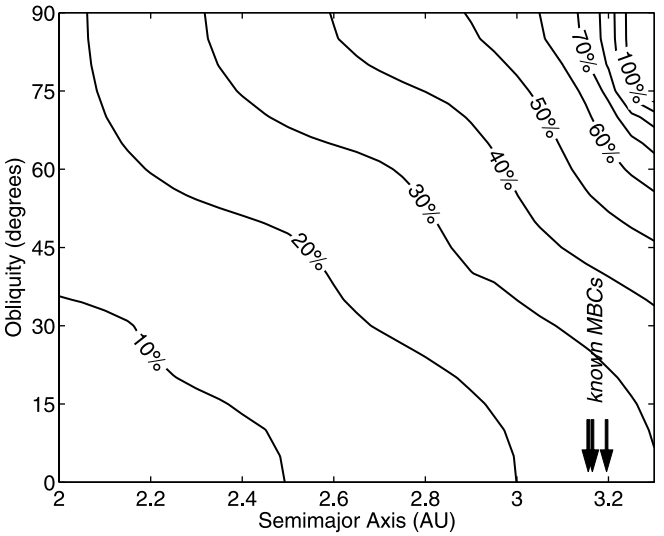

FIG. 5b

FIG. 5.—Contours show the fraction of surface area of a spherical body where the mean temperature is below 145 K. (*a*) "Cold case": $I = 5$ J m^{-2} K^{-1} s$^{-1/2}$, $P_{\rm rot} = 40$ hr, $A = 0.2$, $e = 0$, and $\epsilon = 1$. (*b*) "Warm case": $I = 25$ J m^{-2} K^{-1} s$^{-1/2}$, $P_{\rm rot} = 2$ hr, $A = 0.04$, $e = 0.25$, $\epsilon = 0.9$, and $\Omega = 250°$. An intermediate case is shown in Fig. 4.

Impacts can lead to stirring of the surface layer, as observed on the Moon where overturning is estimated at 1 m Gyr^{-1} (Heiken et al. 1991). Similar values might also apply to asteroids. Our calculations assume an already dry surface layer and impact gardening is not considered; they will be unaffected by gardening as long as the impacts do not cause significant heating at the depth of the ice interface.

The one-dimensional thermal model neglects lateral heat flux, whose size we now estimate. The lateral heat flux on a small object is $Q_L = -k\partial T/\partial y$, where y is horizontal distance. Judging by Figure 3, we may take a temperature gradient of 50 K per radian of latitude as typical. The thermal conductivity of pure ice is orders of magnitudes larger than that of dry dust, and we conservatively take it to be 4 W m^{-1} K^{-1}. On a kilometer-sized object, this amounts to a net flux of 4 W m^{-1} K^{-1} $\times$ 50 K/(π500 m) $\approx$ 0.1 W m^{-2}, which is small compared to the incoming solar flux.

We consider ice-rich bodies where the weight of a fully covering dust mantle is greater than the gas pressure difference through the mantle. For example, for a nonrotating body of radius $R = 1$ km and uniform density $\rho = 1000$ kg m^{-3}, the bottom pressure of a surface layer of thickness $\Delta z = 1$ m is $G\rho^2(4\pi/3)R\Delta z = 0.2$ Pa, which is orders of magnitude more than the extremely low equilibrium vapor pressure at 145 K. Hence, at the relevant temperatures, the vapor pressure of H_2O is unable to destroy or disturb the surface layer through the force it exerts. (Although it must be mentioned that Elst-Pizarro is close to being torn apart by centrifugal force.)

5. CONCLUSIONS

The gradual loss of ice from bodies in the main asteroid belt and with orbits typical for the main belt can be calculated in simple ways. Among the parameter dependencies, temperature is the most important. This ultimately leads to the concept of a "shallowly buried snow line," which can be approximately defined by the mean surface temperature below which ice will remain within the top few meters of the surface over the age of the solar system. When the surface layer has a mean molecular free path or grain

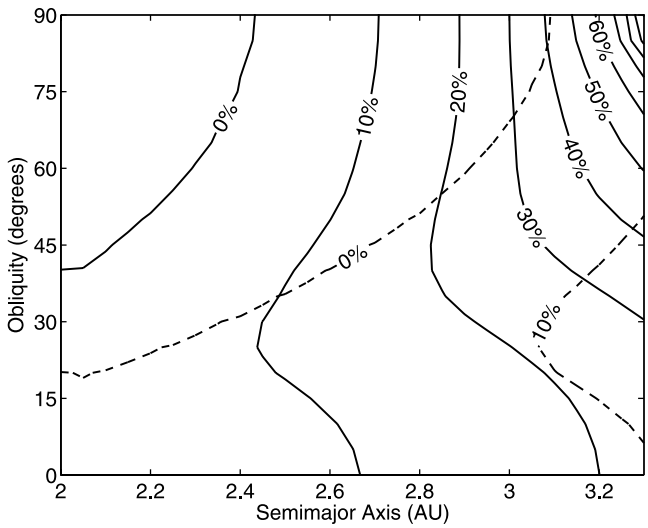

FIG. 6.—Fraction of surface area colder than 145 K (*solid contours*) and 130 K (*dashed contours*) for the same parameters as in Fig. 4, but a thermal inertia of 200 J m^{-2} K^{-1} s$^{-1/2}$. Parameter regions for ice longevity are much smaller.

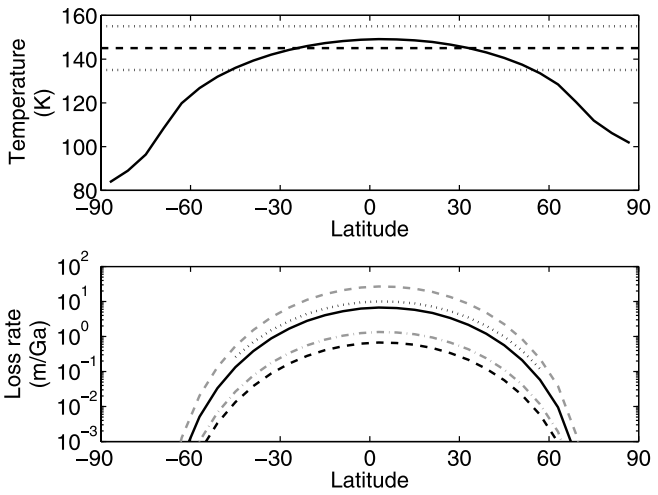

FIG. 7.—Mean temperature and loss rate for a spherical body with the orbital elements and rotation period of 7968 Elst-Pizarro. The thermal inertia is assumed to be 10 J m^{-2} K^{-1} s$^{-1/2}$ and the obliquity 20°. In the top panel, the temperature range 135–155 K is indicated by horizontal dotted lines. Parameters for the lines in the bottom panel are as in Figure 1.

size on the order of 0.1 mm, this temperature is estimated to be about 145 K. A variation of 10 K up or down captures an enormous range of realistic parameters for the physical properties of the surface layer. A threshold of about 145 K applies to dusty surfaces, while that for rocky surfaces with a longer molecular free path can be significantly lower.

Realistic temperature estimates reveal a large parameter space where subsurface ice is long-lasting, as indicated in Figure 4, as long as the surface layer is dusty. Temperatures can be low enough for ground ice to survive over the age of the solar system in all of the main belt, but preferentially for large distances, slowly rotating bodies, low thermal conductivity, and for spin axes roughly aligned with the orbital plane.

Approximately speaking, we have considered the loss rate of ice as a function of about a dozen parameters: surface layer thickness, grain size, equilibrium vapor pressure measurements and ice phase, porosity, tortuosity, semimajor axis, orbital eccentricity, obliquity of the rotation axis, latitude, albedo, emissivity, rotation rate, and thermal inertia. Exploratory and systematic calculations show that ice should be able to persist on many main belt bodies. In conclusion, if the snow line was so close to the Sun that icy bodies formed in the main asteroid belt or if icy bodies were delivered to the main belt, then this snow line is still to be found buried beneath the surfaces of many of these objects.

It is a pleasure to thank Nader Haghighipour, Troy Hudson, Dave Jewitt, Karen Meech, and Dina Prialnik for insightful discussions.

REFERENCES

Baragiola, R. A. 2003, Planet. Space Sci., 51, 953
Britt, D. T., Yeomans, D., Housen, K., & Consolmagno, G. 2002, in Asteroids III, ed. W. F. Bottke, et al. (Tucson: Univ. Arizona Press), 485
Bryson, C. E., Cazcarra, V., & Levenson, L. L. 1974, J. Chem. Eng. Data, 19, 107
Cremers, C. J., & Birkebak, R. C. 1971, in Proc. Sec. Lun. Sci. Conf., Vol. 3, ed. A. A. Levinson (Cambridge: MIT Press), 2311
Evans, R. B., Watson, G. M., & Mason, E. A. 1961, J. Chem. Phys., 35, 2076
Fanale, F. P., & Salvail, J. R. 1984, Icarus, 60, 476
———. 1989, Icarus, 82, 97
Groussin, O., et al. 2007, Icarus, 187, 16
Hardy, B. 1998, in Papers and Abstracts from the Third International Symposium on Humidity and Moisture (Teddington: National Physical Laboratory)
Heiken, G. H., Vaniman, D. T., & French, B. M. 1991, Lunar Sourcebook: A User's Guide to the Moon (Cambridge: Cambridge Univ. Press)
Hsieh, H. H., & Jewitt, D. C. 2006, Science, 312, 561
Hsieh, H. H., Jewitt, D. C., & Fernández, Y. R. 2004, AJ, 127, 2997
Hudson, T. L., Aharonson, O., Schorghofer, N., Farmer, C. B., Hecht, M. H., & Bridges, N. T. 2007, J. Geophys. Res., 112, E05016
Jenniskens, P., Blake, D. F. & Kouchi, A. 1998, in Solar System Ices, ed. B. Schmitt, et al. (Dordrecht: Kluwer), 139
Jones, T. D., Lebofsky, L. A., Lewis, J. S., & Marley, M. S. 1990, Icarus, 88, 172
Kouchi, A. 1987, Nature, 330, 550
———. 1990, J. Crystal Growth, 99, 1220
Kryszczynska, A., La Spina, A., Paolicchi, P., Harris, A. W., Breiter, S., & Pravec, P. 2007, Icarus, 192, 223
Langseth, M. G., Keihm, S. J., & Peters, K. 1976, in Proc. 7th Lunar Sci. Conf., ed. D. C. Kinsler (New York: Pergamon), 3143
Lebofsky, L. A., & Spencer, J. R. 1990, in Asteroids II, ed. R. P. Binzel, T. Gehrels, & M. S. Matthews (Tucscon: Univ. Arizona Press), 128
Ledlow, M. J., Burns, J. O., Gisler, G. R., Zhao, J.-H., Zeilnik, M., & Baker, D. N. 1992, ApJ, 384, 640
Mason, E. A., & Malinauskas, A. P. 1983, Gas Transport in Porous Media: The Dusty-Gas Model (Amsterdam: Elsevier)
Mason, E. A., Malinauskas, A. P., & Evans, R. B. 1967, J. Chem. Phys., 46, 3199
McSween, H. Y., Jr., Ghosh, A., Grimm, R. E., Wilson, L., & Young, E. D. 2002, in Asteroids III, ed. W. F. Bottke, et al. (Tucson: Univ. Arizona Press), 559
Pravec, P., Harris, A. W., & Michalowski, T. 2002, in Asteroids III, ed. W. F. Bottke, et al. (Tucson: Univ. Arizona Press), 113
Presley, M. A., & Christensen, P. R. 1997a, J. Geophys. Res., 102, 6535
———. 1997b, J. Geophys. Res., 102, 6551
Prialnik, D., Benkhoff, J., & Podolak, M. 2004, in Comets II, ed. M. C. Festou, H. U. Keller, & H. A. Weaver (Tucson: Univ. Arizona Press), 359
Sack, N. J., & Baragiola, R. A. 1993, Phys. Rev. B, 48, 9973
Schorghofer, N. 2007, Phys. Rev. E , 75, 041201
Schorghofer, N. & Taylor, G. J. 2007, J. Geophys. Res., 112, E02010
Spencer, J. R., Lebofsky, L. A., & Sykes, M. V. 1989, Icarus, 78, 337
Toth, I. 2006, A&A, 446, 333
Vasavada, A. R., Paige, D. A., & Wood, S. E. 1999, Icarus, 141, 179
Ward, W. R. 1974, J. Geophys. Res., 79, 3375
Washburn, E. W., et al. 2003, International Critical Tables of Numerical Data, Physics, Chemistry, and Technology (Norwich: Knovel)
Watson, K., Murray, B. C., & Brown, H. 1961, J. Geophys. Res., 66, 1598